Modeling Seasonal Evolution of Liquid Water Percolation in Maritime and Continental Snowpacks

Justin Matthew Pflug

A thesis
submitted in partial fulfillment of the
requirements for the degree of

Master of Science in Civil Engineering

University of Washington
2018

Committee:
Jessica Lundquist
Bart Nijssen

Program Authorized to Offer Degree:
Civil and Environmental Engineering

University of Washington

Abstract

Modeling Seasonal Evolution of Liquid Water Percolation
in Maritime and Continental Snowpacks

Justin Matthew Pflug

Chair of the Supervisory Committee:
Professor Jessica Lundquist
Civil and Environmental Engineering

Accurate model representation of liquid water percolation through snow is crucial for snowpack runoff forecasts. Here, we investigate model representation of liquid water percolation with both parameter-based and physically-based routines. Routines for these two approaches were implemented within the SnowModel snow evolution framework (Liston and Elder, 2006a) and evaluated against point measurements at two maritime sites in Washington State and one continental site in Colorado, USA. Physically-based simulations improved peak snow depth over 3 meters (79%) with respect to the parameter-based routine in the Olympic Mountains of Washington State. Further, improvements in snowpack root-mean-squared-error (RMSE) and snow disappearance timing were also observed in all domains. The physically-based percolation routine also outperformed the parameter-based percolation routine when using parameter-sets from other climates and snow seasons. However, the Olympic Mountains of Washington, USA contained unique liquid water fluxes that were not fully described by the physically-based routine. We hypothesize that flow in this region exhibits evidence of preferential flow paths

instead of uniform, matric flow and is therefore not transferable between domains given the modeling architecture.

1. Introduction:

For snow models to accurately represent snow state variables across the globe, the model physics must be valid for all climates where snow occurs (Armstrong and Brun, 2008; Liston and Elder, 2006a; Stieglitz et al., 2001). Transferability between climates and the ability to simulate future snow given expected warming may also be compromised for models developed for a particular climate (Tanaka and Tachikawa, 2015). Therefore, physically-based representations of snow and hydrologic processes are advantageous for future snow projections and water supply forecasting in ungauged basins (Hunukumbura et al., 2012; Lidén and Harlin, 2000; van der Linden and Woo, 2003; van Werkhoven Kathryn et al., 2008)

Here we investigate the importance of liquid water percolation and the ability of a snow model to represent processes related to liquid water percolation such as mass-balance, precipitation-phase partitioning, and snow temperature evolution. We investigate this by modifying a widely-implemented snow model developed and tested primarily in cold regions (Liston and Elder, 2006a, 2006b; Liston and Hiemstra, 2008, 2011a, 2011b). Observations from the Buckinghorse SNOpack TELemetry station (SNOTEL), Snoqualmie Pass snow study site, and Swamp Angel study plot were then utilized to evaluate model performance and the transferability between climates and snow seasons. While we modified a single snow model, the results are important to anyone developing or implementing snow models in regions subject to liquid water fluxes within the snowpack.

This paper is arranged as follows. Section 2 provides pertinent background information on liquid water infiltration, percolation schemes, and physics in commonly used models. Section 3 explains SnowModel, model adjustments, and the percolation theory that was implemented. Section 4 details the modeling domains and data used in this study. Section 5 describes the model simulations, and the results and analyses are included in section 6. Additional discussions and conclusions are presented in Sections 7 and 8, respectively.

2. Background

2.1 Importance of liquid water in snow

Rain, canopy drip, and snow melt all contribute liquid water to snow. Due to relatively high mean winter temperatures, snowpacks in maritime regions are particularly susceptible to mixed-precipitation, canopy drip, and snow melt. In continental or arctic climates, liquid water content and percolation are less common due to reduced liquid sources and low snowpack temperatures. However, warm maritime snowpacks commonly hold non-negligible amounts of water (Fisher et al., 2005; Sturm et al., 1995) often resulting in snow-accumulation-season runoff.

Model representations of liquid water percolation become increasingly important as temperatures increase and percolation processes become more common. Rapid liquid channeling and melt from high temperatures, humidity, and wind during rain on snow events often result in largescale flooding (Christner and Harr, 1982; Harr, 1981; Leavesley, 1997; Marks et al., 1998, 2001; McCabe et al., 2007; Rössler et al., 2014; Singh et al., 1997; Wayand et al., 2015). In mountainous regions, high liquid content also poses avalanche hazards (Conway and Abrahamson, 1984; Conway and Raymond, 1993; Schneebeli, 2004; Techel and Pielmeier, 2011). In arctic regions, rain on snow events and freeze-thaw cycles create soil-surface icing which reduce wildlife accessibility to food (Putkonen and Roe, 2003; Tyler, 2010). Liquid water

content also alters snowpack accumulation and affects the timing of snow disappearance, therefore altering water supplies, transportation infrastructure, flora blooming periods, and wildlife behavior.

2.2 Model percolation processes

To compare model percolation process representations, several models were selected from the literature. Choices were initially filtered to frequently-used models (defined by the number of Google Scholar citations) under the criteria that snowpack liquid percolation was represented in some fashion. A further subset of these models was subjectively made to include a combination of hydrologic models (DHSVM, SUMMA), climate land-surface models (Noah-MP), and snow models (SnowModel, SNOWPACK, UEB, Snow-17) with varying architectures. An overview of these models can be found in Table 1.

Model processes of importance to liquid percolation include the snowpack layer-development scheme, energy-balance approach, precipitation partitioning method, and the numerical solver (Table 1). Model layering ranged between single-layer (Snow-17, SnowModel, UEB) and variable-layer schemes (SnowModel, SNOWPACK, SUMMA). DHSVM (Wigmosta et al., 2002, 2010) and Noah-MP (Niu Guo-Yue et al., 2011; Yang and Niu, 2003) also presented set-number layering schemes. Liquid flow within the snowpack is highly heterogeneous and preferential, depending on local snowpack density and the location of buried ice channels and lenses (Albert and Perron, 2000; Colbeck and Anderson, 1982; Conway and Benedict, 1994; Eiriksson et al., 2012; Harrington and Bales, 1998; Kattelmann and Dozier, 1999; Leroux and Pomeroy, 2016; Marsh, 1988; Marsh and Woo, 2008; Singh et al., 1997; Techel and Pielmeier, 2011; Waldner et al., 2004; Webb et al., 2018). Therefore, explicit representation of layers has been recommended for models that are able to resolve storm-layer stratigraphy and evolution (Hirashima et al., 2010). However, for single-layer models, or models with lumped layers, methods posed by Colbeck and Anderson (1982), and adopted in some form by SUMMA (Clark et al., 2015a) and UEB (Tarboton and Luce, 1996), are able to represent percolation by modeling liquid water saturation and treating the snow within a layer as a homogeneous unit (Colbeck and Anderson, 1982).

Liquid water content and percolation rely on the energy-balance solution of snow temperature. All snowpacks are subject to liquid percolation at times when snow bulk-snowpack temperature approaches 0°C. However, warmer maritime snowpacks achieve percolation frequently throughout the duration of the snow season, stressing the importance of accurate snow temperature modeling. All surface energy-balance processes for the models in Table 1 were derived a similar differential relationship,

$$c_s \rho_w h \frac{dT_s}{dt} = \frac{dQ_{cc}}{dt} = Q_{sn} + Q_{ln} + Q_h + Q_e + Q_p + Q_g \qquad (1)$$

where the change in the snowpack cold content (Q_{cc}) is equal to the summed energy for a given timestep (dt). Energies include net shortwave radiation (Q_{sn}), net longwave radiation (Q_{ln}), sensible heat (Q_h), latent heat (Q_e), heat advected from precipitation (Q_p), and the ground heat flux (Q_g). The energy calculation for each component on the right-side of Equation 1 varied

Table 1. Frequently-used model physics. Processes shown were determined to be important for liquid flux processes. Red and Blue lines in the precipitation partitioning section represent linear and stepwise partitions, respectively.

Model	Layering	Surface energy-balance					Precipitation partition	Numerical solver					Percolation scheme				
		Atmosphere-skin interaction	Liquid-water refreezing	Conduction between layers	Force-restore	Parameterized		Forward finite-difference	Tri-diagonal matrix solver	Newton-Raphson method	Finite-element method	Euler predictor-corrector	Parameterized water threshold	Snow energy refreezing	Pore-space thresholding	Capillary physics	Gravity liquid drainage
DHSVM (Wigmosta et al., 2002; Wigmosta et al., 2010)	2-layer	X	X				Linear	X					X	X			
Noah-MP (Niu Guo-Yue et al., 2011; Yang and Niu, 2003)	3-layer	X	X	X			Step or Linear		X						X		
Snow-17 (Anderson, 1976)	Single-layer					X	Step or User-defined	X					X				
SnowModel (Liston and Elder, 2006; Liston et al., 1999)	Single-layer	X					Step			X			X				
	Multilayer	X	X	X					X	X			X				
SNOWPACK (Lehning et al., 2002; Hirashima et al., 2010)	Multilayer	X	X	X			User-defined				X					X	
SUMMA (Clark. et al., 2015a, 2015b)	Multilayer	X	X	X			Step or Linear			X							X
UEB (Tarboton and Luce, 1996)	Single-layer				X		Linear					X					X

significantly between models. Further, ground heat fluxes and heat advected by precipitation are not always included in the energy-balance solution. Readers are directed to the sources included in Table 1 for further information. The energy balance is also sensitive to the model layering scheme. For example, multilayer schemes often resolve sporadic melt events more accurately than single-layer schemes, due to reduced thermal inertia at upper-snowpack layers (Dutra et al., 2011). The change in snowpack cold content denoted by the product of heat capacity (c_s), snow water equivalent ($\rho_w h$), and change in snowpack temperature ($\frac{dT_s}{dt}$), were solved with different numerical solving schemes (Table 1). While the numerical solving scheme was not changed for this study, it is important to note that differences in numerical and time-stepping methods can result in non-negligible differences between model solutions (Clark and Kavetski, 2010; Kavetski and Clark, 2010).

The liquid percolation routine varied significantly between the seven models (Table 1). The most physically-based method was found in SNOWPACK, where capillary forces between layers of modeled stratigraphy were accounted for (Hirashima et al., 2010; Lehning et al., 2002; Wever et al., 2014). In SUMMA and UEB, snow temperature, liquid water content, ice content, and density are used to calculate snowpack relative saturation and the resulting drainage with respect to gravity (Clark et al., 2015a; Colbeck, 1972, 1974; Colbeck and Anderson, 1982; Tarboton and Luce, 1996). Noah-MP, SnowModel, and Snow-17 (Anderson, 1976) percolate water via a threshold defined by snow pore space, liquid holding-capacity, and density, respectively. Unlike the rest of the models in Table 1, DHSVM contains two different percolation routines for the thin surface layer and the underlying snowpack. All models except Snow-17, UEB, and SnowModel's single-layer framework account for the latent release of energy from refreezing of liquid water in the snowpack.

Uncertainty in precipitation amount and phase remains a dominant source of modeling error (Currier et al., 2017; Jennings et al., 2018; Marks et al., 2013; Wayand et al., 2016, 2017). This is particularly troublesome for percolation routines reliant on accurate representations of liquid water input. Among the models in Table 1, stepwise or linear thresholds based on air, dew point, or wet-bulb temperatures are the most common. However, user-defined methods allow for the explicit definition of solid and liquid precipitation into the modeling framework using observations, atmospheric models, or topographic-based relationships.

3 Percolation theory and model selection

3.1 Model and percolation routine selection

SnowModel is a variable-layer, distributed model with robust representations of distributed meteorology, incoming energy, and snowpack evolution. In complex mountainous terrain, SnowModel's ability to redistribute snow with wind (Hiemstra et al., 2002; Liston and Sturm, 1998; Liston et al., 2007), account for radiative differences between slopes (Liston et al., 1999; Sproles et al., 2013), redistribute avalanching snow (Bernhardt and Schulz, 2010), derive glacier melt (Mernild et al., 2006, 2007), and calculate runoff routing (Liston and Mernild, 2012) all provide unique advantages.

To date, SnowModel has been used primarily in arctic or continental regions. Therefore, SnowModel as originally coded, resolved ablation-season runoff well but was unequipped for warm temperatures and high volumes of accumulation season runoff observed in the Olympic Mountains of Washington, USA. This resulted in abnormally deep snow depth and late runoff

(Figure1). However, Currier et al. (2017) accurately modeled the evolution of SWE in the same maritime climate using SUMMA employed with the gravity-drainage routine. While SUMMA simulations modeled runoff at a variety of snow densities, SnowModel's snowpack liquid infiltration scheme only modeled runoff at periods with density exceeding a maximum density threshold, thus missing runoff during the accumulation season.

To better resolve liquid water transport, SnowModel was altered to include a more physically-based percolation routine. The gravity-drainage theory (Colbeck and Anderson, 1982) employed within the SUMMA framework was chosen as the physically-based percolation routine for this study. In addition to providing favorable results in the Olympic Mountains, the gravity-drainage percolation routine was generally compatible with SnowModel's state variables and layering framework. SnowModel's percolation routine is also isolated entirely within the snow-evolution subroutine (SnowPack) making model changes straightforward. The added infiltration scheme is detailed in Section 3.2 below.

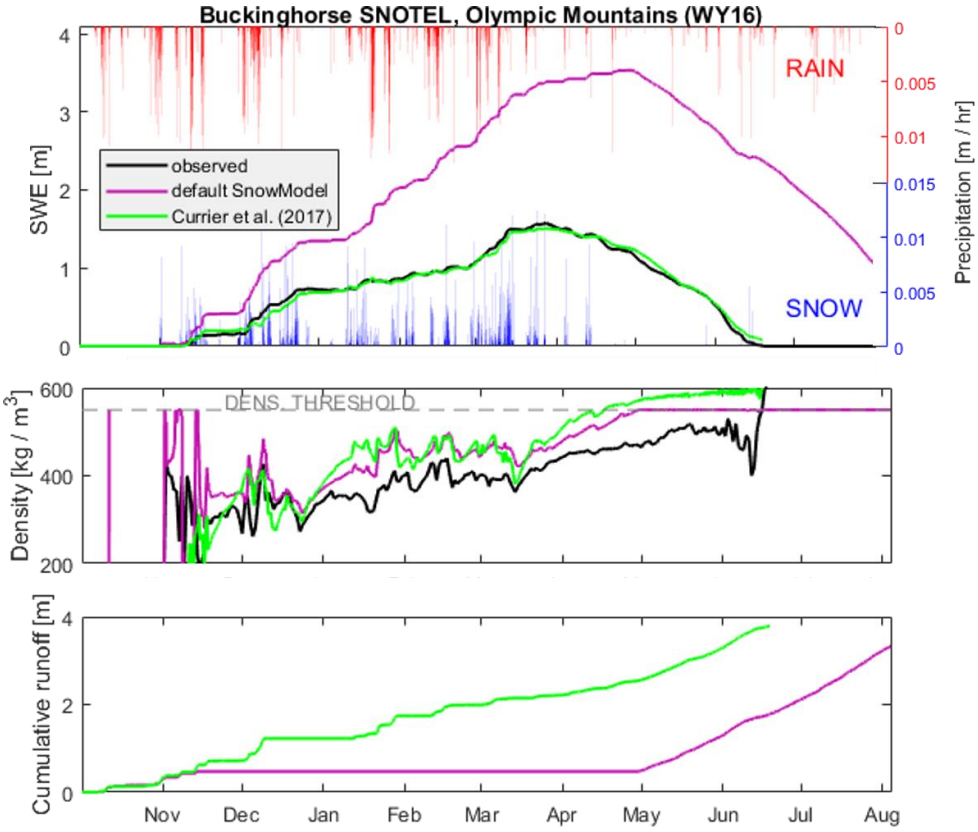

Figure 1. SnowModel simulations of SWE (top), bulk-snowpack density (middle), and cumulative runoff (bottom) are compared to observations and simulations performed by Currier et al., (2017) in the Olympic Mountains for water year 2016. The density-threshold used to drive runoff in the default SnowModel framework is shown by the dashed-gray line (middle).

3.2 Gravity-drainage theory

Liquid water presence in the snowpack creates large, bonded clusters, which reduces capillary forces and initiates flow predominantly due to gravity (Brun, 1989; Colbeck and Anderson, 1982). Saturated flow can be approximated by,

$$q_g = -K_{sat} * R^{MW} \quad (2)$$

where $-K_{sat}$ is the saturated hydraulic conductivity (in units of length per time) and R is the relative saturation (fractional and unitless). The meltwater exponent (MW) is a fitting-parameter derived from field observations but is typically equal to 3.0 with little sensitivity (Colbeck and Anderson, 1982). The sign of the hydraulic conductivity represents an imposed coordinate system with negative fluxes in the direction of gravity.

For a snow layer or snowpack of a known temperature (T), the fraction of snowpack water in the liquid-state can be represented by the freezing point temperature (T_f) and a user-defined freezing curve parameter (ξ) ranged between 10 and 1000 (Clark et al., 2015b; Jordan, 1991).

$$\varphi_{liq} = \frac{1}{1+\left(\xi*(T_f-\min(T,T_f))\right)^2} \quad (3)$$

$$\theta_{liq} = \varphi_{liq} * \rho_s \quad (4)$$

$$\theta_{ice} = \left(1-\varphi_{liq}\right) * \rho_s * \left(\frac{\rho_w}{\rho_{ice}}\right) \quad (5)$$

The volumetric fractions of liquid water (Equation 4) and ice (Equation 5) are derivable for modeled snow density (ρ_s), defined water density (ρ_w) ($1000\ kg/m^3$), and defined ice density (ρ_{ice}) ($917\ kg/m^3$). The volumetric fraction of air, or pore space (θ_{air}), is then the fractional amount required for $\theta_{liq} + \theta_{ice} + \theta_{air} = 1$. The residual water content, or percent of the pore-space that can be filled prior to releasing fluxes, can then be parameterized by a capillary retention parameter (F_{cap}) and modeled pore space.

$$\theta_{resid} = F_{cap} * \theta_{air} * \omega \quad (6)$$

irreducible content multiplier (ω) ranges between 1 and 0 and decreases exponentially for ice densities greater than $550\ kg/m^3$, thus reducing the amount of water that can be held in dense, ice-filled layers.

Equations 2 through 6 use snowpack density following compaction processes and snow temperatures from the previous timestep. Liquid available to transport is then determined within the model timestep by,

$$\theta_{tran} = \theta_{liq} + (rain + drip_{can} + melt)/depth_h \quad (7)$$

where $depth_h$ is the depth of the snowpack (for single-layer simulations) or first snow-layer (for multilayer simulations). In other words, θ_{tran} represents the volume fraction of liquid water within the snowpack. If θ_{tran} exceeds θ_{resid} for a given timestep, fully-saturated snow properties are simulated, and fluxes occur according to Equation 3. The relative saturation (fraction ranging between 0 and 1) is then the ratio of the remaining liquid water and remaining air space after pore-space filling,

$$R = \frac{\theta_{tran} - \theta_{resid}}{\theta_{air} - \theta_{resid}}. \quad (8)$$

For multilayer simulations, θ_{resid} and θ_{tran} are calculated for every layer, from the top of the snowpack to the bottom, with the layer influx equal to the flux out of the overlaying layer.

4 Modeling Domains and Data

4.1. Buckinghorse SNOTEL

Observations of daily snow depth and snow water equivalent collected by the National Resources Conservation Service (NRCS) Buckinghorse SNOTEL were used to evaluate model performance. We focused on water-year 2016 because it represented the median annual SWE accumulation, with somewhat average meteorological conditions. Further, Currier et al. (2017) was able to reproduce Buckinghorse snow depth and SWE using SUMMA to high accuracy (Figure 1) and provided a trusted model to compare the SnowModel simulations against.

Buckinghorse is located within a topographic saddle above the Elwha watershed (elevation 1484 m.) centralized in the Olympic Mountain Range of Northwest Washington State. This site commonly receives 2.5 – 3.0 meters of annual water-equivalent precipitation with snowpack often exceeding 4 meters in depth. While 80% of the precipitation in this region typically occurs between October and March, temperate conditions caused 40% of the precipitation in water year 2016 to fall between the temperatures of -1° and 2°C (Currier et al., 2017). Between October and April 1st, Buckinghorse observed 2.27 meters of precipitation at air temperatures above 0°C (Figure 2).

Northwest Modeling Consortium (Mass et al., 2003) Weather Research and Forecasting (WRF) model runs were used to force simulations at Buckinghorse. Atmospheric models provide data for sites without forcing data as opposed to meteorological extrapolations. While SnowModel partitions rain and snow based on a stepwise temperature threshold (Table 1), WRF allows for microphysical-depictions of snow or rain formation and the evolution of phase while falling through the atmosphere (Thompson et al., 2004, 2008). Analysis of mixed precipitation events and WRF prescription of precipitation phase can be found in the discussion section. While WRF-model biases may have been present for other meteorological variables, WRF-modeled and SNOTEL air temperature appeared to be unbiased. Readers are directed to Currier et al., (2017) for more information regarding WRF Buckinghorse data.

4.2 Snoqualmie Pass

Continuous observations of daily SWE accumulation and hourly bulk snowpack depth at the Snoqualmie Pass snow study site (elevation 921 m.) were collected by the Washington Department of Transportation avalanche team and University of Washington Mountain Hydrology team during water year 2013 and 2014. Precipitation, relative humidity, near-surface air temperature, and near-surface wind speed were also observed by a meteorological station within the snow plot. Lysimeter data is also provided at this site, although runoff quantity is expected to be error-prone (Wayand et al., 2017).

Over a meter of precipitation was observed at air temperatures above 0°C between October and March at Snoqualmie (Figure 2). Although still considered a maritime climate, cold air intrusions from eastern Washington result in high variability in air temperature.

4.3 Swamp Angel

The Swamp Angel Study Plot (SASP) is in the Colorado Rocky Mountains within the Senator Beck Basin (elevation 3370 m.). To focus on the process of liquid water percolation, Swamp Angel was specifically chosen since winds speeds are low and processes of wind redistribution are less likely to bias observations. Low temperatures and clear-sky conditions result in relatively high incoming shortwave radiation and minimized incoming longwave radiation (Figure 2). As opposed to Buckinghorse and Snoqualmie, only 0.04 m of precipitation occurred for temperatures over 0° C between October and March of water year 2015.

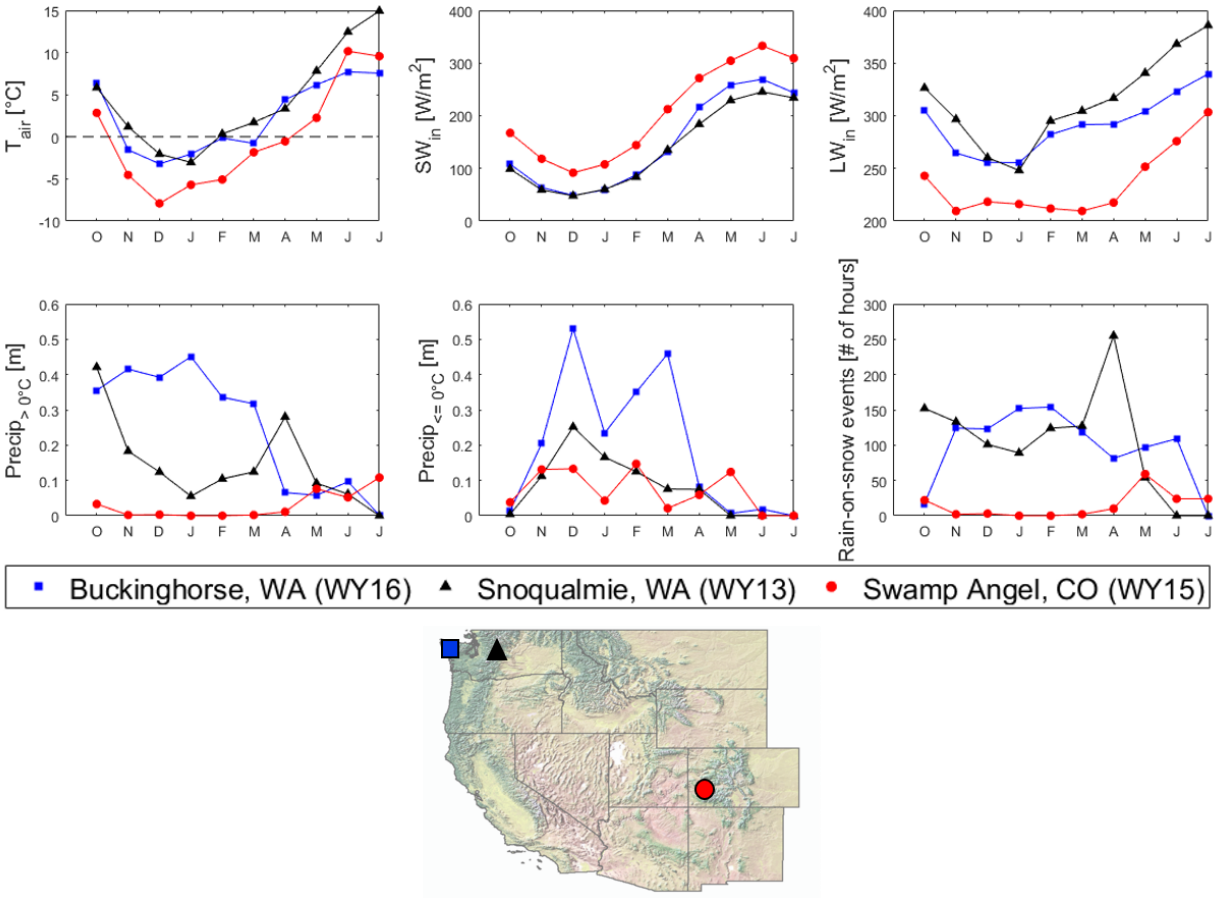

Figure 2. Meteorological conditions for Buckinghorse, WA (blue, square), Snoqualmie, WA (black, triangle), and Swamp Angel, CO (red, circle) for WY16, WY13, and WY15 respectively. Plots of air temperature, incoming shortwave radiation, and incoming longwave radiation are monthly averages while precipitation at all temperatures and the number of rain on snow events are monthly sums. The number of rain-on-snow events is approximated by the number of rain events occurring at air temperatures greater than 0°C (in hours).

5 Methods

5.1 SnowModel alterations

While both single and multilayer SnowModel simulations track snow depth, SWE, snow density, and runoff, the method of calculation and order of calculations are not identical. Further, layers are reduced and merged throughout the sublimation and melting processes in multilayer model runs. Therefore, the order in which water is added or removed from the snowpack is important for percolation. The resulting model framework and placement of additional model subroutines are depicted in Figure 3. In both single and multilayer frameworks, the added routines replace SnowModel's default runoff process with runoff from the total liquid flux (single-layer) or liquid flux out of the bottom snowpack layer (multilayer).

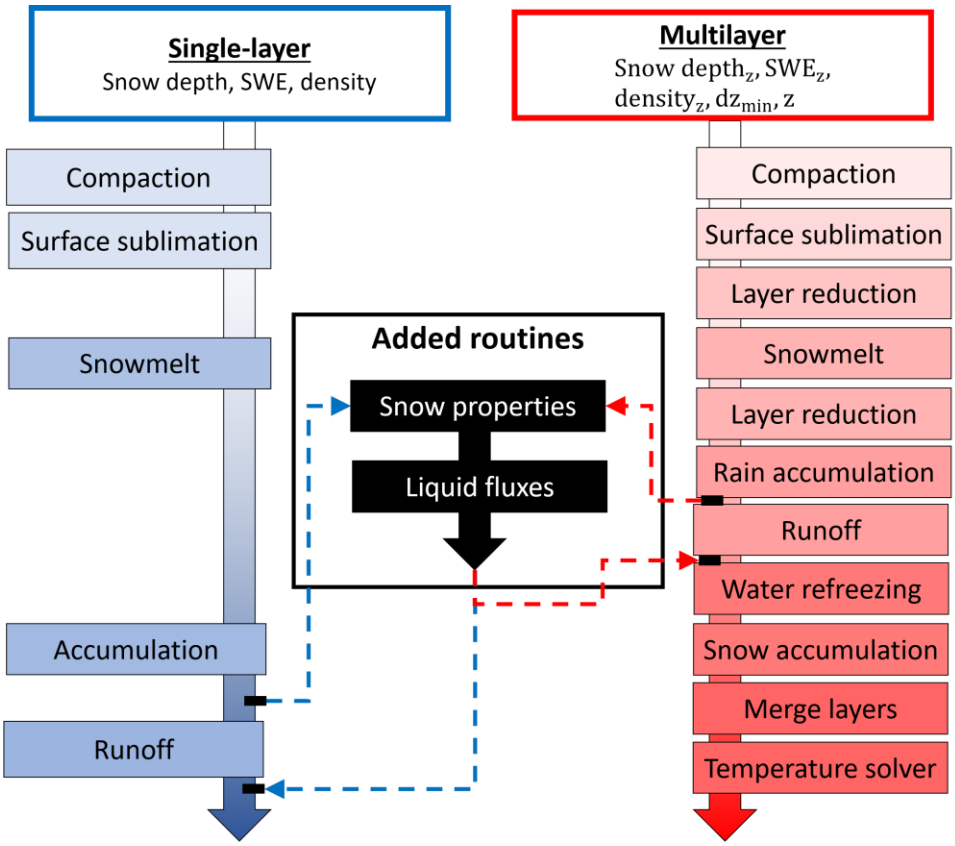

Figure 3. SnowModel single-layer (blue) and multilayer (red) snowpack frameworks are sequentially ordered from top to bottom. Additional model routines added in this study are shown in black. Similar processes between the layering schemes are aligned vertically. Note that runoff and accumulation occur at different times in single and multilayer simulations and are therefore not vertically aligned like the other processes. In both scenarios, the added routines replace existing SnowModel runoff.

For the multilayer routine, snow temperatures from the previous timestep are assumed to be representative of the snowpack temperature at the beginning of the current timestep. This was therefore used to determine the snowpack liquid and ice content (Equations 3 – 5) prior to warming or cooling of the snowpack throughout the current timestep. In multilayer simulations,

latent heat release from liquid water freezing is also included. The increase in snow temperature (restricted to the freezing point) can be shown by,

$$\Delta T_z = \frac{\varphi_{liq} * L_f}{c_s * dy_{snow}} \quad (9)$$

where L_f is the latent heat of fusion for ice (~334 Joules per gram) and dy_{snow} is the thickness of the layer the liquid flux travels into. Upon the completion of the timestep, a finite control-volume methodology and tri-diagonal matrix solver is used to simultaneously solve for all layer temperatures given the step's energy balance (Baliga and Patankar, 1980; Liston et al., 1999).

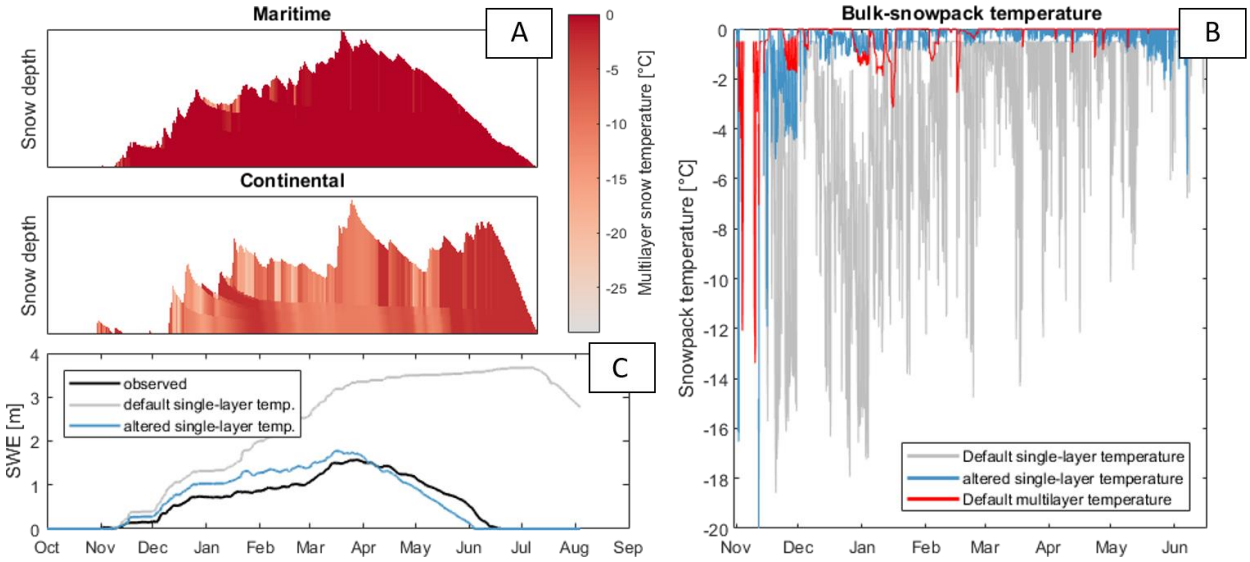

Figure 4. Multilayer SnowModel runs provided realistic representations of snow temperature in both maritime and continental climates (A). However, single-layer simulations resulted in a snowpack that was far too cold in maritime regions (B). Since the added gravity-drainage scheme was sensitive to snow temperature (Equation 3), realistic results were only achieved by employing a temperature damping curve for single-layer simulations (C).

For single-layer SnowModel simulations, the bulk-snowpack temperature was originally the average between the snow-surface temperature and a constant ground-surface temperature of -1°C. This resulted in erroneously low snowpack temperature (Figure 4b). In fact, the highest possible bulk-snowpack temperature was -0.5°C, resulting in less than 1% liquid water content under all freezing curve parameterizations (Equation 3). In the original single-layer modeling framework, snow temperature was only used for snowpack compaction routines and was realistic for arctic and continental regions. However, gravity-drainage percolation is highly sensitive to snow temperature and necessitated the inclusion of a new single-layer snow temperature routine.

Maritime snowpack approaches 0°C at shallower depths (Sturm et al., 1995) resulting in a nonlinear temperature-depth relationship. Therefore, a temperature damping-depth relationship for soil heat fluxes proposed by Bhumralkar, (1975) was adapted for single-layer SnowModel simulations (Figure 5),

$$T_s(z) = \overline{T_s} + \Delta T_{surf} e^{-\frac{z}{d}} \quad (10)$$

where $\overline{T_s}$ is the average bulk snowpack temperature and ΔT_{surf} is the difference between the average snowpack temperature ($\overline{T_s}$) and the modeled snowpack surface temperature. The exponential increase of snow temperature for a given depth (z) is then scaled by a damping depth, or depth in which the snow-surface temperature no longer affects the snow temperature,

$$d = \left(\frac{2\gamma}{\frac{c_s \rho}{dt}}\right)^{\frac{1}{2}} \quad (11)$$

where γ is the snow thermal conductivity and ρ is snow density. The resulting bulk-snowpack temperature is then,

$$T_{bulk} = \frac{-\int_{h_s}^{0} T_s(z)dz}{h_s} \quad (12)$$

where h_s is the snowpack depth. Use of the snowpack single-layer damping depth reduced the mean temperature bias from -3.27 to -0.15°C compared to multilayer simulations at Buckinghorse (Figure 4b). Warmer modeled snowpack and higher liquid water contents were then able to release runoff more efficiently using the gravity-drainage routine and produced an improved match with the observations (Figure 4c).

The single-layer temperature routine solves for snow temperature using the snow surface temperature independently at each timestep. This assumes that the snowpack comes to thermal equilibrium during the course of the current timestep. Further, the single-layer temperature routine does not include latent heat release for liquid water refreezing. Therefore, changes in bulk snowpack temperature from one timestep to the next result in unaccounted changes in snowpack cold content (Equation 1) and errors in the energy-balance.

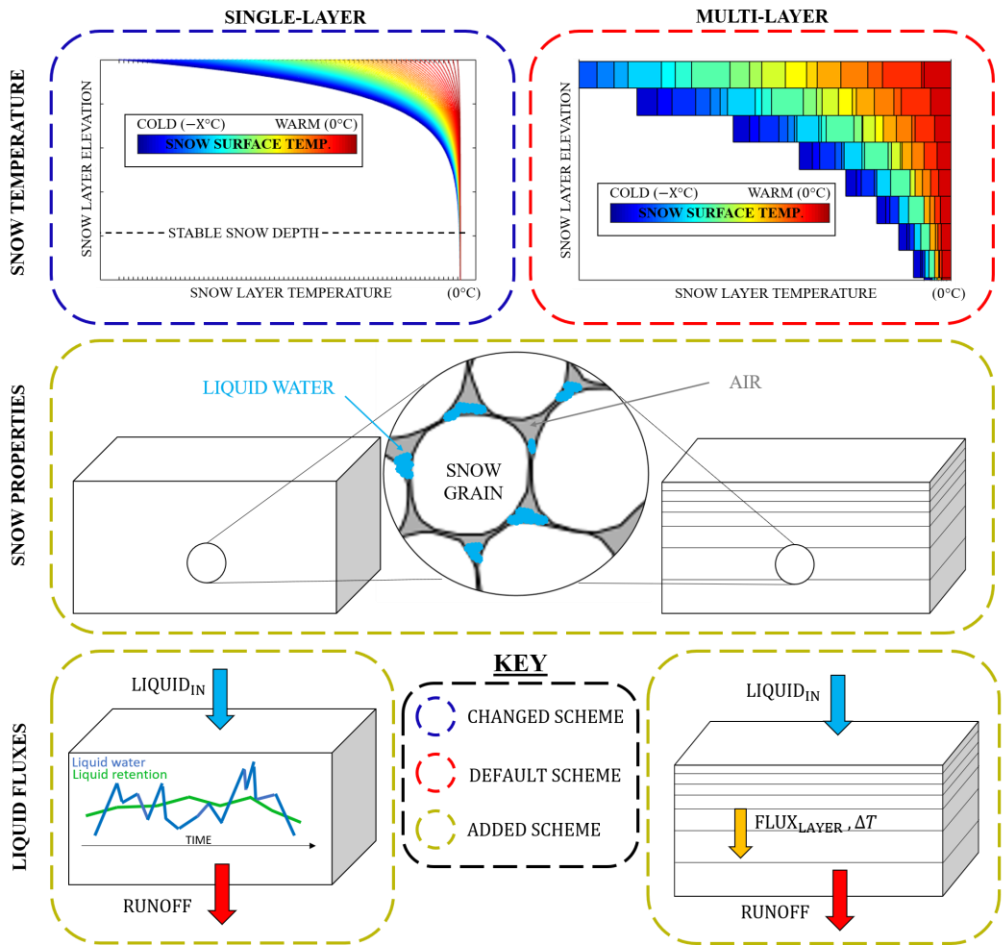

Figure 5. Gravity-drainage model changes and additions. The snow-properties routine remained identical between single-layer and multilayer routines (middle). However, latent heat release from liquid fluxes in the multilayer routine altered snow temperature (bottom). The default temperature evolution routine was used for multilayer simulations, while a damping depth curve (Equation 10) was applied for single-layer simulations (top).

5.2 Locally-calibrated simulations

To configure SnowModel simulations, default SnowModel parameters had to be calibrated. Albedo and critical temperature parameters were initially uncertain due to errors in the default model runs. For this reason, albedo, albedo decay, and critical temperature for all three domains were derived from the literature and remained unchanged throughout the duration of this study. Albedo used by Sproles et al. (2013) in the maritime Oregon Cascades agreed closely with parameters from Currier et al. (2017) in the Olympic Mountains. New snow albedo was therefore set to 0.80, decaying at 0.018 day^{-1} and 0.008 day^{-1} for melting and cold conditions respectively, at both Snoqualmie and Buckinghorse. Albedo at the Swamp Angel Study Plot was instead selected within the bounds observed by Skiles and Painter (2017). This selection resulted in identical albedo decay with a new snow albedo of 0.84. The critical temperature, or the temperature that partitioned liquid and solid precipitation, was defined as 0°C for all domains. Simulations were also performed for hourly timesteps for all of the domains.

The addition of the gravity-drainage routine in SnowModel introduced multiple parameters. These included the freezing curve parameter (Equation 4), hydraulic conductivity (Equation 3),

capillary retention (Equation 7), and meltwater exponent (Equation 3). To achieve the best fit to the observations, a semi-automated calibration routine was created to test parameter combinations for the variables listed in Table 2. The calibration was constrained for multiple metrics of general interest to the snow community including root-mean-squared-error (RMSE), peak SWE/snow-depth error (PSDE), peak-snow timing (PST), and snow disappearance timing (SDT). Simulations were then given a normalized score between 0 and 1, with the scale ranging between perfect performance (score of 1) and the model that performed the worst for a given metric (score of 0). Weighting each metric evenly by simply summing the scores, the simulations with the highest gross score represent the models that performed the best as a whole.

5.3. Model transferability simulations

A purely physically-based snow model should be able to model snowpack evolution in a variety of climates throughout multiple snow seasons, with a single calibrated parameter-set. Alternatively, locally-calibrated simulations from Section 5.2 represent idealized scenarios. Tests from section 5.2 were therefore analyzed in order to select a simulation that best appeared to represent the snowpack evolution. This parameter-set was then applied to all of the domains. Multi-year records at the Snoqualmie snow station were also used to test model transferability at a single site between two years. To compare against simulations from Section 5.2, the parameter-set was calibrated for water year 2014 and applied to water year 2013.

6 Results

6.1. Default model simulations

Default SnowModel simulations performed poorly for Buckinghorse (Figure 1 and Figure 6a). While SUMMA simulations (Currier et al., 2017) released intermittent runoff at a variety of snow densities, SnowModel's simulated runoff began in late April at times when the maximum density threshold (550 kg/m^3) was exceeded (Figure 1 and Figure 7). Although SnowModel and SUMMA simulated densities agreed closely, Buckinghorse accumulated deep snowpacks and was therefore capable of retaining large amounts of rain and melt without achieving maximum density. While Sproles et al. (2013) reproduced favorable SnowModel results by reducing the maximum snow density to 330 kg/m^3 in the Oregon Cascades, snow density in the Olympic Mountains can reach 550 kg/m^3 and would be restricted to incorrect densities if lowered. This would, therefore, adversely impact any process combing measured snow depth and modeled snow density to derive SWE.

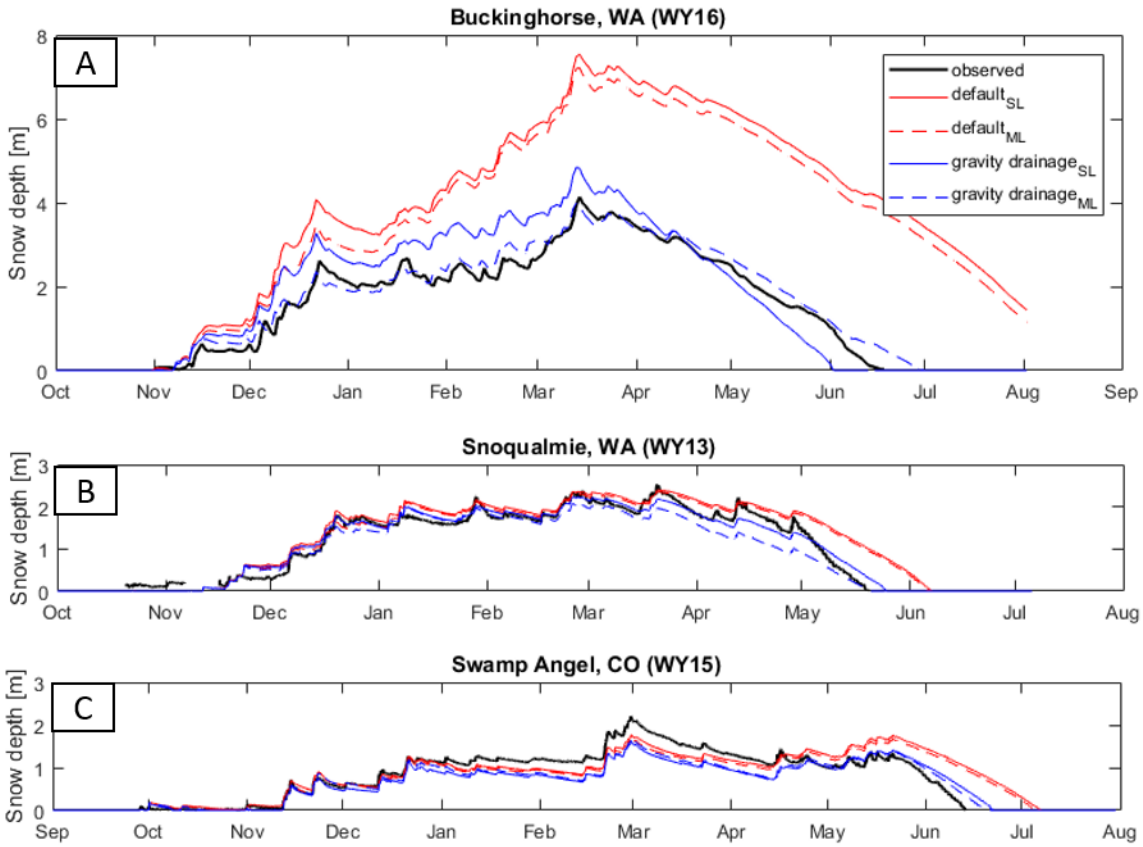

Figure 6. Default and gravity-drainage modeled snow depth are compared to observations for both single-layer (SL) and multilayer (ML) simulations. Y-axes are scaled with respect to one another to highlight the deep snow at Buckinghorse. The dates between the domains correspond to different years (marked in the plot titles).

Differences between default single and multilayer simulations (Figure 6) were a function of the energy-balance solution and the resulting snow temperature. This, in turn, impacts the multilayer processes of compaction, latent heat release from refreezing, and conduction between layers. However, the net effects on modeled SWE were minor. While default multilayer simulations resulted in reduced snow depths, reductions were consistently less than 10% of the single-layer depth for all three domains.

Late and low-biased runoff during the ablation season resulted in late melt-out dates for all domains (Figure 6). While ablation-season runoff was able to be adjusted by altering albedo parameters, calibration degraded model performance with respect to other metrics (RMSE, PSDE, PST).

6.2. Locally-calibrated simulations

Locally-calibrated parameter-sets for the single and multilayer gravity-drainage models are included in Table 2. The freezing curve parameter, used to relate snow temperature to liquid water content (Equation 3), was highly sensitive for gravity-drainage simulations. The capillary retention parameter, responsible for filling the snowpack pore space (Equation 6), also displayed small amounts of sensitivity. The hydraulic conductivity and meltwater exponent (Equation 2) showed little sensitivity and were able to achieve similar results with multiple combinations. It

should be noted that differences in snow temperature between single and multilayer gravity-drainage simulations resulted in different liquid and ice contents, thus requiring different parameterizations for the same domain. Freezing-curve sensitivity is investigated further in Section 7.1.

Table 2. Gravity-drainage parameter-sets. The bolded parameter-set for Snoqualmie multilayer gravity-drainage simulations was also applied to Buckinghorse and Swamp Angel simulations (see Section 6.3).

Domain	*Run*	*Freezing-curve parameter*	*Hydraulic conductivity [m/s]*	*Capillary retention [%]*	*Meltwater exponent*	*Thermal conductivity* $[WK^{-1}m^{-1}]$
Buckinghorse	Single-layer	490	0.013	6	3.0	0.42
	Multilayer	135	0.016	3	3.0	-
Snoqualmie	Single-layer	606	0.012	6	3.0	0.50
	Multilayer	**501**	**0.016**	**6**	**2.9**	-
Swamp Angel	Single-layer	950	0.012	6	3.0	0.55
	Multilayer	681	0.016	5	3.0	-

Note: The freezing curve parameter and meltwater exponent are both dimensionless and used to fit curves for snow temperature and saturated flow, respectively. Multilayer simulations calculate thermal conductivity and therefore do not require a thermal conductivity parameter.

Table 3. Metrics of root-mean-squared-error (RMSE), peak snow/SWE depth error (PSDE), peak snow timing (PST), and snow disappearance timing (SDT). Both single (SL) and multilayer (ML) simulations are presented for both modeling frameworks. Bolded statistics are from simulations using the Snoqualmie multilayer gravity-drainage parameter-set (section 6.3). All other statistics were from idealized simulations where parameter-sets were individually calibrated. All parameter-sets can be found in Table 2.

Domain	*Run*	*RMSE [m]*	*PSDE [m]*	*PST [days]*	*SDT [days]*
Buckinghorse	Default (SL)	2.67 (1.46)	3.40 (1.91)	0 (30)	N/A
	Default (ML)	2.43 (1.38)	3.08 (1.88)	0 (29)	N/A
	Grav. drainage (SL)	0.57 (0.26)	0.70 (0.20)	-1 (-14)	-17 (-17)
	Grav. drainage (ML)	0.22 (0.12)	-0.15 (0.01)	-1 (-2)	11 (11)
	Snoqualmie calibration (ML)	**1.43 (0.83)**	**1.74 (1.01)**	**0 (-1)**	**44**
Snoqualmie	Default (SL)	0.31	-0.13	0	18
	Default (ML)	0.28	-0.18	0	17
	Grav. drainage (SL)	0.14	-0.29	-23	5
	Grav. drainage (ML)	0.23	-0.46	-24	1
Swamp Angel	Default (SL)	0.30	-0.44	0	24
	Default (ML)	0.29	-0.48	0	22
	Grav. drainage (SL)	0.26	-0.58	0	8
	Grav. drainage (ML)	0.22	-0.52	0	6
	Snoqualmie calibration (ML)	**0.23**	**-0.52**	**0**	**-2**

Note: Values in parentheses represent metrics with respect to SWE while all other metrics are with respect to snow depth. PST and SDT are rounded to the nearest day. Simulations were only run 2 months past observed snow disappearance and therefore result in no snow disappearance for Buckinghorse default simulations (Figure 6a).

Model performance varied between default and gravity-drainage simulations (Table 3 and Figure 6). The most significant improvements were seen for Buckinghorse where RMSEs were reduced by 77 and 91% for single and multilayer gravity-drainage simulations, respectively. Further, peak snow depth was improved by nearly 3 meters. While gravity-drainage simulations reduced the RMSE at both Snoqualmie and Swamp Angel, mid-March gravity-drainage simulations resulted in the mistiming of peak snow depth at Snoqualmie and therefore increased peak snow depth error. At Swamp Angel, peak snow depth error was also increased for gravity-drainage simulations. However, no runoff occurred at Swamp Angel during the accumulation season for any model framework (Figure 7), and the cumulative sublimation was nearly zero. Assuming that observations were valid and unbiased, this suggests that errors in compaction contributed to snow depth error at Swamp Angel. While default simulations only released runoff once the maximum density had been achieved, multilayer gravity-drainage runoff timing occurred for densities of 492 kg/m^3 on average, ranging between 353 kg/m^3 and 631 kg/m^3($\pm$ 2 standard deviations).

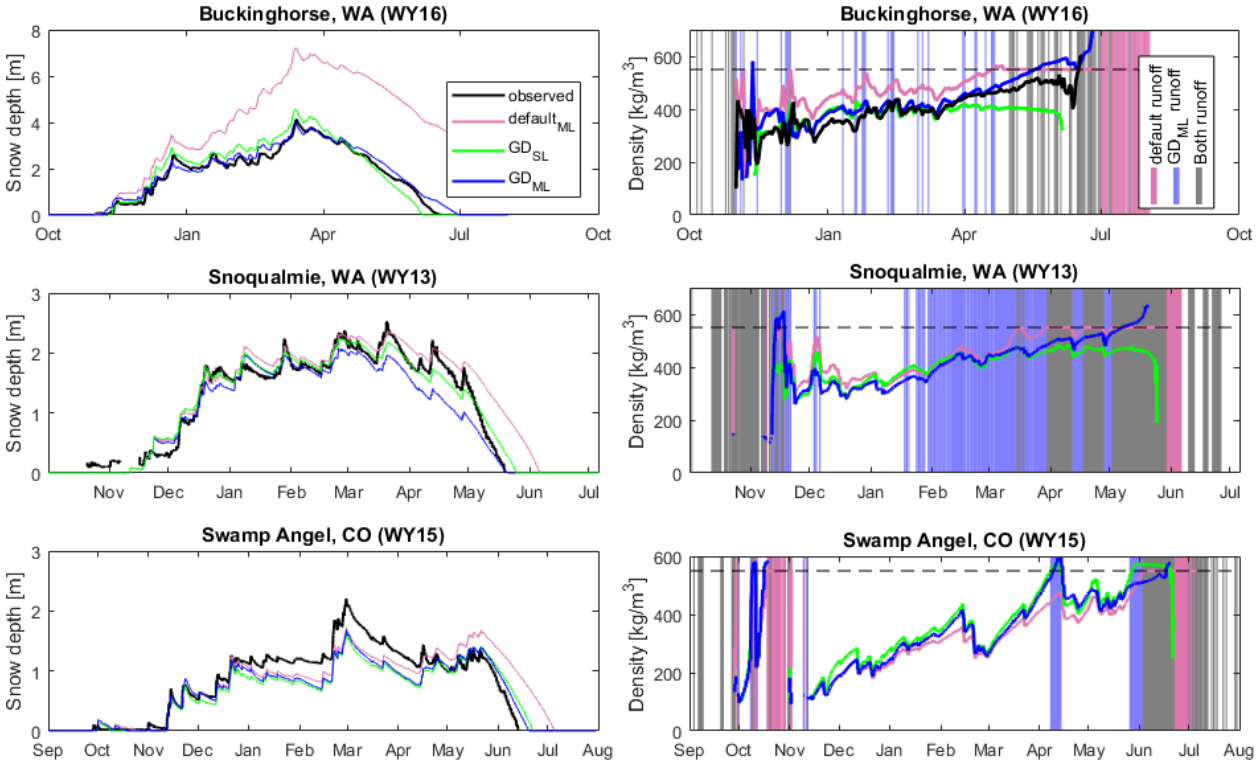

Figure 7. Modeled snow depth (left) and density evolution (right) are compared between simulations and observations. Vertical bars in the density plots are color-coded based on the model framework and represent times at which runoff of any amount occurred. Note that runoff events are only depicted for the default multilayer simulation (pink) and the gravity-drainage multilayer simulation (blue). Also note that y-axes and the simulation dates are also different between subplots.

Both gravity-drainage and default SnowModel simulations were unable to resolve a lysimeter-observed runoff event at Snoqualmie between 7, January and 11, January 2013. While small amounts of rain and melt provided approximately 0.07 m of liquid water throughout this time, gravity-drainage and default simulations displayed very different sensitivities. Only 0.01 m of additional liquid water would have been required for gravity-drainage simulations to resolve

melt. However, default simulations required an additional 0.31 m of liquid water to achieve maximum density and model runoff, therefore indicating that gravity-drainage models are more suited to resolve sporadic runoff events.

Liquid precipitation and accumulation-season melt can cause differences between the timing of peak snow depth and peak SWE. Buckinghorse observations identified peak snow depth on March 15, 2016, 14 days prior to peak SWE (Figure 8). Over this 14-day period, 0.19 m of precipitation fell, with 0.04 m falling at temperatures above 0°C. This combination of meteorological factors reduced the snow depth by 0.51 m and accumulated 0.07 m of SWE. While single and multilayer gravity-drainage simulations agreed with density observations closely, only the multilayer model was able to resolve the timing of both the peak snow depth and peak SWE (Table 2 and Figure 8).

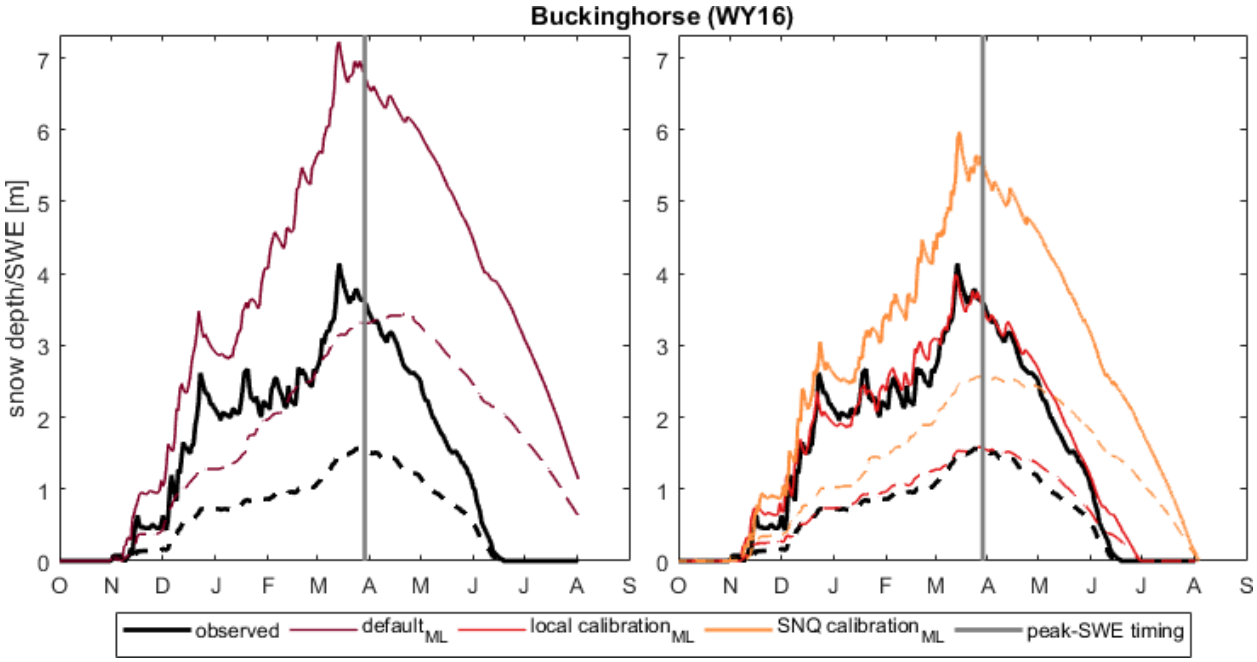

Figure 8. Snow depth (solid) and SWE (dashed) are shown for default (purple), locally-calibrated gravity-drainage (red), Snoqualmie-calibrated gravity-drainage simulations (orange). All simulations were multilayer. While gravity-drainage peak SWE simulations align with the observed peak SWE timing (gray bar), peak SWE occurs 29 days late for default simulations. Peak snow depth is within a day of observed peak snow depth for all simulations and observations.

6.3 Model transferability

Parameters may be calibrated to incorrect values to overcome errors in the model physics. For example, parameters at Swamp Angel may have been calibrated in an attempt to counteract errors in snowpack compaction and retain deeper snow depth. Large differences in the freezing curve parameter at Buckinghorse also suggested that this parameter was accounting for processes that were not present at the other two domains (Section 7.1). Due to this, and the exceptional fit to Snoqualmie depth observations (Section 6.2), the Snoqualmie multilayer gravity-drainage parameter-set was chosen as the parameter-set of use for climate transferability studies at both Buckinghorse and Swamp Angel.

Varied performance was observed for simulations employed with the Snoqualmie multilayer parameter-set (Table 3). Although residing in very different climates (Figure 2), Swamp Angel

simulations with the Snoqualmie parameter-set saw only a 0.01 m increase in RMSE but a 4-day improvement in snow disappearance timing with respect to the locally-calibrated multilayer gravity-drainage simulation. Buckinghorse simulations with the Snoqualmie parameter-set resulted in less-ideal simulations with an RMSE 0.83 m in SWE. However, Buckinghorse simulations using the Snoqualmie parameter-set outperformed default simulations in every category. Further, peak SWE and snow depth timing were both resolved (Figure 9).

Model transferability in time was tested at Snoqualmie for water year 2013 with calibration performed in water year 2014 (Table 4). As compared to locally-calibrated simulations in water year 2013, RMSE and peak snow depth error improved by 0.06 and 0.22 m, respectively. However, this resulted in 13-day increase in snow disappearance timing.

Table 4. Metrics of root-mean-squared-error (RMSE), peak snow depth error (PSDE), peak snow timing (PST), and snow disappearance timing (SDT) for multilayer gravity drainage and default models. Bolded statistics represent the calibrated model run.

Year	*Run*	*RMSE [m]*	*PSDE [m]*	*PST [days]*	*SDT [days]*
WY 2013	Default (ML)	0.25	-0.18	1	17
	Grav. drainage (ML)	0.17	-0.24	0	14
WY 2014	Default (ML)	0.10	-0.08	0	2
	Grav. drainage (ML)	**0.09**	**-0.12**	**0**	**0**

Note: Gravity-drainage calibration was performed for WY2014 alone. The calibrated parameters are as follows: freezing curve = 600, hydraulic conductivity = 0.010 m/s, capillary retention = 7%, and meltwater exponent = 3.0.

7. Discussion

7.1 Buckinghorse percolation processes

Buckinghorse simulations displayed high sensitivity to the freezing curve parameter. This was a result of altered snowpack ice content, pore space, and the resulting liquid holding capacity θ_{resid} (Equation 6). In fact, peak snow depth was increased approximately 0.71 m for every 100-increment increase in the freezing curve parameter. For the same increments, Snoqualmie and Swamp Angel displayed significantly reduced sensitivity, increasing by only 0.14 m and 0.01 m, respectively. This sensitivity either indicated that: 1) the relationship between the freezing curve parameter and snow liquid water content was physically different in this domain, or 2) flow was occurring, or being biased, with respect to a different percolation process.

Buckinghorse simulations did not include canopy cover and were not subject to canopy drip. Therefore, liquid water sources included rain precipitation, snow melt, and liquid content as a function of snow temperature and density (Equations 3 and 4). However, when adapting SnowModel's liquid flux framework to exclude rain precipitation and melt when calculating transferable liquid water (Equation 7), very little sensitivity was seen. This indicated that high sensitivity in the freezing curve parameter was a product of only liquid precipitation and melt.

Simulations using the locally-calibrated and Snoqualmie-calibrated parameter-sets were compared to each other at Buckinghorse (Figure 9). While rain (explicitly defined by WRF) and melt totals were identical in periods when both simulations modeled snowpack, the amount of runoff released from the modeled snowpack was very different. Results found that rain

precipitation was strongly correlated to modeled runoff for locally-calibrated simulations. In fact, most modeled runoff during high-volume rain events was greater than the rain event itself. This indicated that all liquid precipitation, and additional amounts of melt, were likely being released to runoff. Alternatively, for simulations employing the Snoqualmie parameter-set, increased amounts of retention were modeled for both precipitation and melt events, causing overaccumulation as compared to observations.

Since multilayer SnowModel processes include layer merging, heterogeneities like ice lenses and drainage channels are not preserved. For this reason, preferential flow was neglected, and uniform flow through homogeneous layers was modeled. However, retention of rain precipitation at Buckinghorse was rare, therefore suggesting the presence of drainage channels. Buckinghorse may have been particularly susceptible due to the high amount of rain on snow. Although estimated Buckinghorse rain events occurred only 4 days more frequently than Snoqualmie rain events throughout November – March, the precipitation amount averaged 3.9 times larger on average (Figure 2). Therefore, rain magnitude and frequency, along with relatively high snowpack temperatures, were likely sufficient to create drainage channels capable of routing rain precipitation to runoff at Buckinghorse. This same phenomena was also seen in the maritime California Sierra Nevada mountains where large amounts of rainfall on wet, maritime snow resulted in flooding but very little change in SWE at local snow pillows (Dettinger et al., 2009). Additionally, heat advected from liquid precipitation appeared to be biased low, resulting in cold-biased snowpack temperatures. This also required freezing curve parameters to be reduced to promote snowpack runoff.

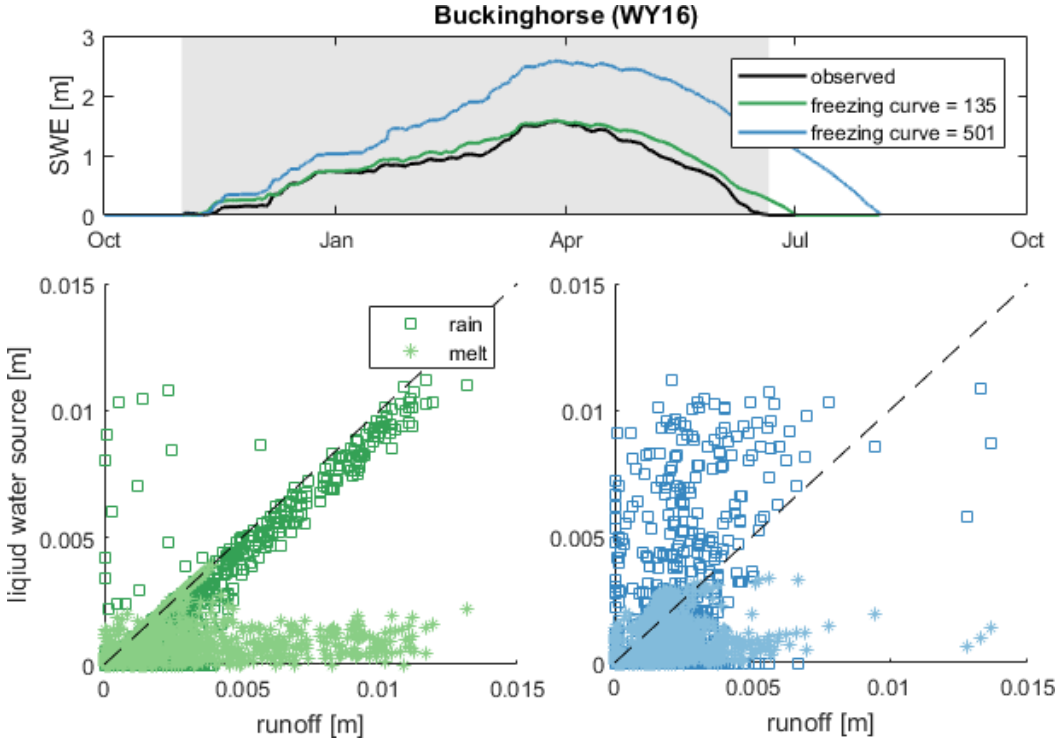

Figure 9. Relationships between rain (boxes) and melt (stars) liquid water sources are compared to runoff amounts using the locally-calibrated parameter-set (green) and the Snoqualmie-calibrated parameter-set (blue). Regressions (bottom) were performed for periods when snow was present in both simulations and observations (gray, top) therefore ensuring that melt and rain precipitation were identical. All points right of the 1:1 line represent mixed rain and melt events.

7.2 Sensitivity analysis

For all previous simulations, WRF total precipitation at Buckinghorse was partitioned into either solid or liquid precipitation with a stepwise function about a critical air temperature of 0°C. However, WRF determined that 44% of periods with precipitation at Buckinghorse during water year 2016 contained mixed precipitation. SnowModel's multilayer framework (Figure 3) was adapted to include mixed precipitation events. This implementation assumed that rain precipitation is incident to the previous snowpack surface and is not absorbed by the snow accumulating throughout the mixed event (see order of model operations in Figure 3). When using the locally-calibrated parameter-set, the Buckinghorse multilayer gravity-drainage SWE RMSE was reduced an additional 21% with a four-day improvement in the melt-out timing, when mixed-precipitation percentages from WRF were used as input to SnowModel.

Multilayer gravity-drainage simulations were also highly sensitive to the number of layers employed in the model (Figure 10). Gravity-drainage simulations at Buckinghorse modeled increased levels of liquid water retention for reduced numbers of layers. Increased accumulation was due to thicker snow depths, increased thermal inertia, and colder snowpacks. However, increasing or decreasing the maximum number of layers resulted in mixed effects for Swamp Angel simulations. This was attributed to the varied magnitude of small runoff events and the resulting density from merging layers. While significant deviations in model simulations were observed as early as December for Buckinghorse simulations, Swamp Angel simulations remained insensitive until late into the snow season when runoff first occurred.

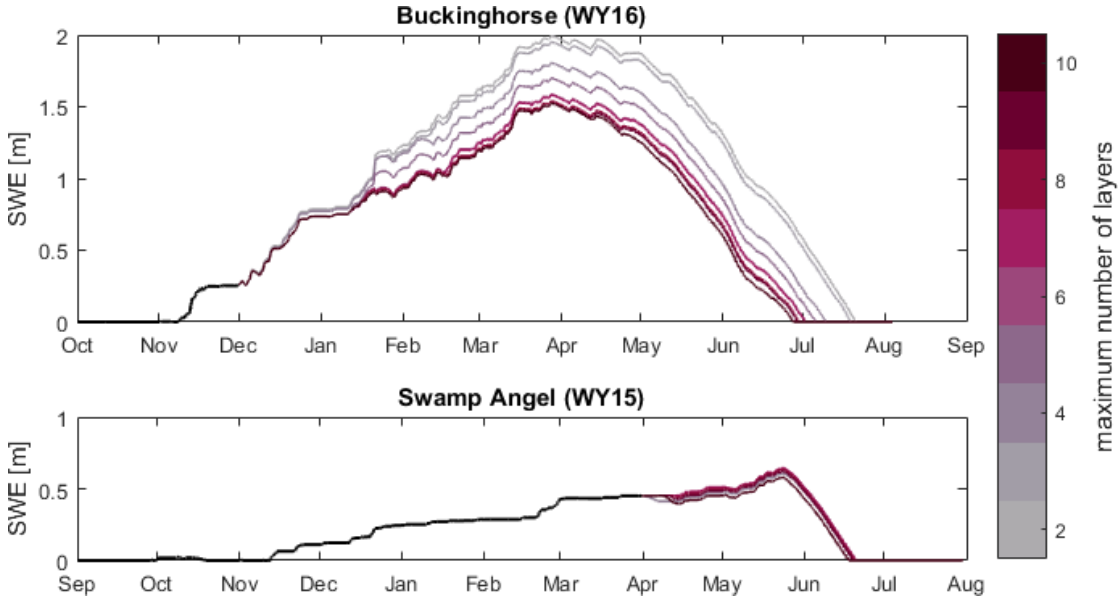

Figure 10. Layer-sensitivity for Buckinghorse and Swamp Angel multilayer gravity-drainage simulations. Both Buckinghorse and Swamp Angle simulations were able to resolve at least 10 snow layers at peak-snow. Therefore, the sensitivity test was constrained between 2 and 10 layers.

7.3 Assumptions and special cases

Several assumptions were applied throughout this study. Due to SnowModel processes, flow was assumed to represent a uniform, matrix wetting front. However, evidence of drainage

channeling at Buckinghorse resulted in significant modeling errors given calibration in another domain. SnowModel simulations were also performed at gridded elevations, meaning that each gridcell has a surface perpendicular to gravity at some user-defined resolution. However, for steep slopes, percolation will not travel downward with respect to the snowpack normal, but rather in the direction of gravity, resulting in increased percolation lengths. Buried ice lenses also promote lateral water transport, therefore altering snow mass-balance from inter-gridcell fluxes. Depending on the snow properties and hydraulic conductivity, liquid percolation can be gradual. However, gravity-drainage simulations assume the completion of drainage within a given timestep. Therefore, increased errors may be seen for short model timesteps. Finally, gravity-drainage alterations assumed saturated flow was the only process capable of initiating runoff. While saturated flows are the most dominant source of percolation, unsaturated flow from capillary physics between layers of different properties may be present in deep snowpacks.

8. Conclusion

Snowpack runoff is a function of liquid water saturation rather than density. This is particularly true in maritime climates, where liquid-water sources of rain and melt are common throughout both the accumulation and ablation season. Physically-based percolation routines are therefore required to accurately model runoff and snow evolution across multiple climates and between snow seasons with inter-annual variability.

At the Buckinghorse SNOTEL station, locally-calibrated gravity-drainage simulations resulted in a 91% improvement in SWE RMSE and a 1.9-meter improvement in peak-SWE as compared to density-threshold simulations. Snow disappearance timing and snow depth RMSE were also improved for all three model domains, including a continental-climate snow station. Gravity-drainage simulations were able to resolve runoff events in response to melt and liquid precipitation for a range of densities, therefore better matching observations and improving the representation of snowpack evolution. While improvements were seen for both single and multilayer gravity-drainage frameworks, multilayer simulations better resolved the snowpack energy balance and resulting timing of peak SWE.

Snoqualmie simulations calibrated for water year 2014 outperformed density-threshold simulations in water year 2013. Further, in comparing model simulations between climates, gravity-drainage simulations calibrated for Snoqualmie performed better than density-threshold simulations for both the Buckinghorse and Swamp Angel snow stations. While gravity-drainage simulations were highly transferable between the Snoqualmie maritime and Swamp Angel continental climates, Buckinghorse simulations required a unique parameterization. This was likely due to preferential flow that occurred at Buckinghorse, but not as frequently at the other sites.

9. Acknowledgements

We gratefully acknowledge funding support from the University of Washington Valle Scholarship and Scandinavian Exchange Program, the National Park Service Future Park Leaders of Emerging Change (FPL), NASA grant NNX17AL59G, and NASA grant NNX14AJ72G. We would also like to thank Neal Johnson for providing access to the WRF data archive. The author would also like to express his gratitude to SnowModel developer, Glen Liston, who assisted with model training and insight throughout the duration of this project.

10. Sources

Albert, M.R., and Perron, F.E. (2000). Ice layer and surface crust permeability in a seasonal snow pack. Hydrol. Process. *14*, 3207–3214.

Anderson, E.A. (1976). A point energy and mass balance model of a snow cover. NOAA Tech Rep *N WS 19*, 150.

Armstrong, R.L., and Brun, E. (2008). Snow and climate: physical processes, surface energy exchange and modeling (Cambridge: Cambridge University Press).

Baliga, B.R., and Patankar, S.V. (1980). A New Finite-Element Formulation for Convection-Diffusion Problems. Numer. Heat Transf. *3*, 393–409.

Bernhardt, M., and Schulz, K. (2010). SnowSlide: A simple routine for calculating gravitational snow transport. Geophys. Res. Lett. *37*, L11502.

Bhumralkar, C.M. (1975). Numerical Experiments on the Computation of Ground Surface Temperature in an Atmospheric General Circulation Model. J. Appl. Meteorol. *14*, 1246–1258.

Brun, E. (1989). Investigation on Wet-Snow Metamorphism in Respect of Liquid-Water Content. Ann. Glaciol. *13*, 22–26.

Christner, J., and Harr, R.D. (1982). Peak streamflows from the transient snow zone, western Cascades, Oregon. In Proceedings of the 50th Annual Western Snow Conference, p. 38.

Clark, M.P., and Kavetski, D. (2010). Ancient numerical daemons of conceptual hydrological modeling: 1. Fidelity and efficiency of time stepping schemes. Water Resour. Res. *46*.

Clark, C., Martin P., Nijssen, B., Lundquist, J.D., Kavetski, D., Rupp, D.E., Woods Ross A., Freer Jim E., Gutmann Ethan D., Wood Andrew W., Brekke Levi D., et al. (2015a). A unified approach for process-based hydrologic modeling: 1. Modeling concept. Water Resour. Res. *51*, 2498–2514.

Clark, M.P., Nijssen, B., Lundquist, J.D., Kavetski, D., Rupp, D.E., Woods Ross A., Freer Jim E., Gutmann Ethan D., Wood Andrew W., Gochis David J., et al. (2015b). A unified approach for process-based hydrologic modeling: 2. Model implementation and case studies. Water Resour. Res. *51*, 2515–2542.

Colbeck, S.C. (1972). A Theory of Water Percolation in Snow. J. Glaciol. *11*, 369–385.

Colbeck, S.C. (1974). Water Flow Through Snow Overlying an Impermeable Boundary. Water Resour. Res. *10*, 119–123.

Colbeck, S.C., and Anderson, E.A. (1982). The permeability of a melting snow cover. Water Resour. Res. *18*, 904–908.

Conway, H., and Abrahamson, J. (1984). Snow Stability Index. J. Glaciol. *30*, 321–327.

Conway, H., and Benedict, R. (1994). Infiltration of water into snow. Water Resour. Res. *30*, 641–649.

Conway, H., and Raymond, C.F. (1993). Snow stability during rain. J. Glaciol. *39*, 635–642.

Currier, W.R., Thorson, T., and Lundquist, J.D. (2017). Independent Evaluation of Frozen Precipitation from WRF and PRISM in the Olympic Mountains. J. Hydrometeorol. *18*, 2681–2703.

Dettinger, M., Hidalgo, H., Das, T., Cayan, D., and Knowles, N. Projections of Potential Flood Regime Changes in California. 68.

Dutra, E., Viterbo, P., Miranda, P.M.A., and Balsamo, G. (2011). Complexity of Snow Schemes in a Climate Model and Its Impact on Surface Energy and Hydrology. J. Hydrometeorol. *13*, 521–538.

Eiriksson, D., Whit, M., Luce, C.H., Marshall, H.P., Bradford, J., Benner Shawn G., Black Thomas, Hetrick Hank, and McNamara James P. (2012). An evaluation of the hydrologic relevance of lateral flow in snow at hillslope and catchment scales. Hydrol. Process. *27*, 640–654.

Fisher, F.N., King, M.D., and Lee-Taylor, J. (2005). Extinction of UV-visible radiation in wet midlatitude (maritime) snow: Implications for increased NOx emission. J. Geophys. Res. Atmospheres *110*.

Harr, R.D. (1981). Some characteristics and consequences of snowmelt during rainfall in western Oregon. J. Hydrol. *53*, 277–304.

Harrington, R., and Bales, R.C. (1998). Interannual, seasonal, and spatial patterns of meltwater and solute fluxes in a seasonal snowpack. Water Resour. Res. *34*, 823–831.

Hiemstra, C.A., Liston, G.E., and Reiners, W.A. (2002). Snow Redistribution by Wind and Interactions with Vegetation at Upper Treeline in the Medicine Bow Mountains, Wyoming, U.S.A. Arct. Antarct. Alp. Res. *34*, 262–273.

Hirashima, H., Yamaguchi, S., Sato, A., and Lehning, M. (2010). Numerical modeling of liquid water movement through layered snow based on new measurements of the water retention curve. Cold Reg. Sci. Technol. *64*, 94–103.

Hunukumbura, P.B., Tachikawa, Y., and Shiiba, M. (2012). Distributed hydrological model transferability across basins with different hydro-climatic characteristics. Hydrol. Process. *26*, 793–808.

Jennings, K.S., Winchell, T.S., Livneh, B., and Molotch, N.P. (2018). Spatial variation of the rain–snow temperature threshold across the Northern Hemisphere. Nat. Commun. *9*.

Jordan, R. (1991). A One-Dimensional Temperature Model for a Snow Cover: Technical Documentation for SNTHERM.89. (Hanover, NH: Cold Regions Research and Engineering Lab).

Kattelmann, R., and Dozier, J. (1999). Observations of snowpack ripening in the Sierra Nevada, California, U.S.A. J. Glaciol. *45*, 409–416.

Kavetski, D., and Clark, M.P. (2010). Ancient numerical daemons of conceptual hydrological modeling: 2. Impact of time stepping schemes on model analysis and prediction. Water Resour. Res. *46*.

Leavesley, G.H. (1997). Destructive Water: Water-Caused Natural Disasters, Their Abatement and Control (International Association of Hydrological Sciences).

Lehning, M., Bartlet, P., Fierz, C., and Satyawali, P. (2002). A physical SNOWPACK model for the Swiss avalanche warning: Part II. Snow microstructure. Cold Reg. Sci. Technol. *35*, 147–167.

Leroux, N.R., and Pomeroy, J.W. (2016). A 2D model for simulating heterogeneous mass and energy fluxes through melting snowpacks. Cryosphere Discuss *2016*, 1–26.

Lidén, R., and Harlin, J. (2000). Analysis of conceptual rainfall–runoff modelling performance in different climates. J. Hydrol. *238*, 231–247.

van der Linden, S., and Woo, M. (2003). Transferability of hydrological model parameters between basins in data-sparse areas, subarctic Canada. J. Hydrol. *270*, 182–194.

Liston, G.E., and Elder, K. (2006a). A Distributed Snow-Evolution Modeling System (SnowModel). J. Hydrometeorol. *7*, 1259–1276.

Liston, G.E., and Elder, K. (2006b). A meteorological distribution system for high-resolution terrestrial modeling (MicroMet). J. Hydrometeorol. *7*, 217–234.

Liston, G.E., Haehnel, R., Sturm, M., A Hiemstra, C., Stuefer, S., and D. Tabler, R. (2007). Instruments and Methods Simulating complex snow distributions in windy environments using SnowTran-3D.

Liston, G.E., and Hiemstra, C.A. (2008). A Simple Data Assimilation System for Complex Snow Distributions (SnowAssim). J. Hydrometeorol. *9*, 989–1004.

Liston, G.E., and Hiemstra, C.A. (2011a). Representing Grass– and Shrub–Snow–Atmosphere Interactions in Climate System Models. J. Clim. *24*, 2061–2079.

Liston, G.E., and Hiemstra, C.A. (2011b). The Changing Cryosphere: Pan-Arctic Snow Trends (1979–2009). J. Clim. *24*, 5691–5712.

Liston, G.E., and Mernild, S.H. (2012). Greenland Freshwater Runoff. Part I: A Runoff Routing Model for Glaciated and Nonglaciated Landscapes (HydroFlow). J. Clim. *25*, 5997–6014.

Liston, G.E., and Sturm, M. (1998). A snow-transport model for complex terrain. J. Glaciol. *44*, 498–516.

Liston, G.E., Winther, J.-G., Bruland, O., Elvehøy, H., and Sand, K. (1999). Below-surface ice melt on the coastal Antarctic ice sheet. J. Glaciol. *45*, 273–285.

Marks, D., Kimball, J., Tingey, D., and Link, T. (1998). The sensitivity of snowmelt processes to climate conditions and forest cover during rain-on-snow: a case study of the 1996 Pacific Northwest flood. Hydrol. Process. *12*, 1569–1587.

Marks, D., Link, T., Winstral, A., and Garen, D. (2001). Simulating snowmelt processes during rain-on-snow over a semi-arid mountain basin. Ann. Glaciol. *32*, 195–202.

Marks, D., Winstral, A., Reba, M., Pomeroy, J., and Kumar, M. (2013). An evaluation of methods for determining during-storm precipitation phase and the rain/snow transition elevation at the surface in a mountain basin. Adv. Water Resour. *55*, 98–110.

Marsh, P. (1988). Flow fingers and ice columns in a cold snowcover (Environment Canada, Ground Water Division, National Hydrology Research Institute).

Marsh, P., and Woo, M. (2008). Meltwater Movement in Natural Heterogeneous Snow Covers. Water Resour. Res. *21*, 1710–1716.

Mass, C.F., Albright, M., Ovens, D., Steed, R., MacIver, M., Grimit, E., Eckel, T., Lamb, B., Vaughan, J., Westrick, K., et al. (2003). Regional Environmental Prediction Over the Pacific Northwest. Bull. Am. Meteorol. Soc. *84*, 1353–1366.

McCabe, G.J., Hay, L.E., and Clark, M.P. (2007). Rain-on-Snow Events in the Western United States. Bull. Am. Meteorol. Soc. *88*, 319–328.

Mernild, S.H., Liston, G.E., Hasholt, B., and Knudsen, N.T. (2006). Snow Distribution and Melt Modeling for Mittivakkat Glacier, Ammassalik Island, Southeast Greenland. J. Hydrometeorol. *7*, 808–824.

Mernild, S.H., Liston, G.E., and Hasholt, B. (2007). Snow-distribution and melt modelling for glaciers in Zackenberg river drainage basin, north-eastern Greenland. Hydrol. Process. *21*, 3249–3263.

Niu Guo-Yue, Yang Zong-Liang, Mitchell Kenneth E., Chen Fei, Ek Michael B., Barlage Michael, Kumar Anil, Manning Kevin, Niyogi Dev, Rosero Enrique, et al. (2011). The community Noah land surface model with multiparameterization options (Noah-MP): 1. Model description and evaluation with local-scale measurements. J. Geophys. Res. Atmospheres *116*.

Putkonen, and Roe (2003). Rain-on-snow events impact soil temperatures and affect ungulate survival. Geophys. Res. Lett. *30*.

Rössler, O.K., Froidevaux, P.A., Börst, U., Rickli, R., Martius, O., and Weingartner, R. (2014). Retrospective analysis of a nonforecasted rain-on-snow flood in the Alps – a matter of model limitations or unpredictable nature? Hydrol. Earth Syst. Sci. *18*, 2265–2285.

Schneebeli, M. (2004). Mechanisms in wet snow avalanche release. In Proceedings ISSMA-2004, International Symposium on Snow Monitoring and Avalanches. Snow and Avalanche Study Establishment, India, Manali, India, pp. 75–77.

Singh, P., Spitzbart, G., Hübl, H., and Weinmeister, H.W. (1997). Hydrological response of snowpack under rain-on-snow events: a field study. J. Hydrol. *202*, 1–20.

Skiles, S.M., and Painter, T. (2017). Daily evolution in dust and black carbon content, snow grain size, and snow albedo during snowmelt, Rocky Mountains, Colorado. J. Glaciol. *63*, 118–132.

Spicer, R. (1986). Glaciers in the Olympic Mountains, Washington -- present distribution and recent variations. University of Washington - unpublished master's thesis.

Sproles, E.A., Rittger, K., Nolin, A.W., and Painter, T.H. (2013). Climate change impacts on maritime mountain snowpack in the Oregon Cascades. Hydrol Earth Syst Sci *17*, 2581–2597.

Stieglitz, M., Ducharne, A., Koster, R., and Suarez, M. (2001). The Impact of Detailed Snow Physics on the Simulation of Snow Cover and Subsurface Thermodynamics at Continental Scales. J. Hydrometeorol. *2*, 228–242.

Sturm, M., Holmgren, J., and Liston, G.E. (1995). A Seasonal Snow Cover Classification System for Local to Global Applications. J. Clim. *8*, 1261–1283.

Tanaka, T., and Tachikawa, Y. (2015). Testing the applicability of a kinematic wave-based distributed hydrological model in two climatically contrasting catchments. Hydrol. Sci. J. *60*, 1361–1373.

Tarboton, D.G., and Luce, C.H. (1996). Utah energy balance snow accumulation and melt model (UEB) (Utah Water Research Laboratory).

Techel, F., and Pielmeier, C. (2011). Point observations of liquid water content in wet snow – investigating methodical, spatial and temporal aspects. The Cryosphere *5*, 405–418.

Thompson, G., Rasmussen, R.M., and Manning, K. (2004). Explicit forecasts of winter precipitation using an improved bulk microphysics scheme. Part I: Description and sensitivity analysis. Mon. Weather Rev. *132*, 519–542.

Thompson, G., Field, P.R., Rasmussen, R.M., and Hall, W.D. (2008). Explicit Forecasts of Winter Precipitation Using an Improved Bulk Microphysics Scheme. Part II: Implementation of a New Snow Parameterization. Mon. Weather Rev. *136*, 5095–5115.

Tyler, N.J.C. (2010). Climate, snow, ice, crashes, and declines in populations of reindeer and caribou (Rangifer tarandus L.). Ecol. Monogr. *80*, 197–219.

van Werkhoven Kathryn, Wagener Thorsten, Reed Patrick, and Tang Yong (2008). Characterization of watershed model behavior across a hydroclimatic gradient. Water Resour. Res. *44*.

Waldner, P.A., Schneebeli, M., Schultze-Zimmermann, U., and Flühler, H. (2004). Effect of snow structure on water flow and solute transport. Hydrol. Process. *18*, 1271–1290.

Wayand, N.E., Lundquist, J.D., and Clark, M.P. (2015). Modeling the influence of hypsometry, vegetation, and storm energy on snowmelt contributions to basins during rain-on-snow floods. Water Resour. Res. *51*, 8551–8569.

Wayand, N.E., Stimberis, J., Zagrodnik, J., Mass, C.F., and Lundquist, J.D. (2016). Improving simulations of precipitation phase and snowpack at a site subject to cold air intrusions: Snoqualmie Pass, WA. J. Geophys. Res. Atmospheres *121*, 9929–9942.

Wayand, N.E., Clark, M.P., and Lundquist, J.D. (2017). Diagnosing snow accumulation errors in a rain-snow transitional environment with snow board observations. Hydrol. Process. *31*, 349–363.

Webb, R.W., Williams, M.W., and Erickson, T.A. (2018). The Spatial and Temporal Variability of Meltwater Flow Paths: Insights From a Grid of Over 100 Snow Lysimeters. Water Resour. Res. *54*, 1146–1160.

Wever, N., Fierz, C., Mitterer, C., Hirashima, H., and Lehning, M. (2014). Solving Richards Equation for snow improves snowpack meltwater runoff estimations in detailed multi-layer snowpack model. Cryosphere Katlenburg-Lindau *8*, 257.

Wigmosta, M.S., Nijssen, B., Storck, P., and Lettenmaier, D.P. (2002). The distributed hydrology soil vegetation model. Math. Models Small Watershed Hydrol. Appl. 7–42.

Wigmosta, M.S., Vail, L.W., and Lettenmaier, D.P. (2010). A distributed hydrology-vegetation model for complex terrain. Water Resour. Res. *30*, 1665–1679.

Yang, Z.-L., and Niu, G.-Y. (2003). The Versatile Integrator of Surface and Atmosphere processes: Part 1. Model description. Glob. Planet. Change *38*, 175–189.